

Long distance coherent tunneling effect on the charge and heat currents in serially coupled triple quantum dots

David M T Kuo^{1,2} and Yia-chung Chang^{3,4}

¹*Department of Electrical Engineering and* ²*Department of Physics,*
National Central University, Chungli, 320 Taiwan

³*Research Center for Applied Sciences,*
Academic Sinica, Taipei, 11529 Taiwan and

⁴ *Department of Physics, National Cheng Kung University, Tainan, 701 Taiwan*

(Dated: October 30, 2018)

Abstract

The effect of long distance coherent tunneling (LDCT) on the charge and heat currents in serially coupled triple quantum dots (TQDs) connected to electrodes is illustrated by using a combination of the extended Hurbbard model and Anderson model. The charge and heat currents are calculated with a closed-form Landauer expression for the transmission coefficient suitable for the Coulomb blockade regime. The physical parameters including bias-dependent quantum dot energy levels, electron Coulomb interactions, and electron hopping strengths are calculated in the framework of effective mass theory for semiconductor TQDs. We demonstrate that the effect of LDCT on the charge and heat currents can be robust. In addition, it is shown that prominent heat rectification behavior can exist in the TQD system with asymmetrical energy levels.

I. INTRODUCTION

Semiconductor quantum dots (QDs) have been advocated to be promising candidates as qubits for the realization of solid state quantum computer due to their long coherent time in charge and spin degrees of freedom in comparison to their counterparts.^{1,2} Many experimental studies have been devoted to the coherent tunneling behavior of serially coupled double quantum dots (DQDs).³ The serially coupled DQDs can be used as a spin filter when the Pauli spin blockade condition is met.³ To scale up quantum registers based on QD arrays, one must have good control on the transport properties of quantum dot arrays. It is expected that serially coupled triple quantum dots (TQDs) can reveal the salient features of the charge transport behavior in quantum dot arrays.⁴⁻⁶ The tunneling current spectra of serially coupled TQDs exhibit an unexpected resonance structure arising from the long distance coherent tunneling (LDCT) between the outer QDs.⁴⁻⁶ The interdot coupling strength decreases exponentially with the separation between QDs. Therefore, the direct coupling strength between the outer QDs of a TQD system, which are separated by a large distance, is vanishingly small. However, it has been demonstrated experimentally in Refs. 4 and 5 that the coherent tunneling coupling between the outer QDs is not negligible due to the middle QD-assisted tunneling, which can be understood from the second-order perturbation theory.⁷

Many theoretical studies have been devoted to the transport properties of TQD systems. Topological effect on the electronic properties of a TQD molecule was investigated in Ref. 8. The authors of Ref. 9 studied the control of spin blockade by ac magnetic field in TQDs. Weymann, Bulka and Barnas investigated the dark states in transport through a triangle TQD.¹⁰ The transport properties of a serially coupled TQD have been studied by the master equation for studying multiple electron spin blockade effect in Ref. 11. However there still lacks a systematic analysis to illustrate the LDCT effect on the tunneling current spectra of the serially coupled TQD junction when the intradot and interdot Coulomb interactions are included.

Besides the qubit aspect, the serially coupled QD arrays can also be used as solid state coolers and power generators at nanoscale, which is important in the integration of quantum device circuits.¹² The understanding of energy transfer and heat extraction of the QD array is also crucial in the implementation of solid state quantum register, because the heat

accumulation will degrade the performance of quantum computation. Unlike electronic nanodevices, it is still a challenge to measure the heat transport in nanoscale structures.¹² Up to date, most researches on the thermoelectric properties of nanostructures connected to electrodes have been restricted to theoretical studies.^{13–28} References 13-18 investigated the optimization of figure of merit of QD junction system in the linear response regime. The non-linear thermoelectric properties of nanostructures including QDs, molecules and the other mesoscopic conductors can lead to attractive applications such as thermal rectifiers, heat engines and thermal spintronics.^{19–28} In this paper, the effect of LDCT on the charge and heat currents of TQD junction system is revealed and analyzed in the presence of intradot and interdot electron Coulomb interactions.

II. FORMALISM

Here we consider nanoscale semiconductor QDs, in which the energy level separations are much larger than their on-site Coulomb interactions and thermal energies. Thus, only one energy level for each quantum dot needs to be considered. An extended Hubbard model and Anderson model are employed to simulate a TQD connected to electrodes. The Hamiltonian of the TQD junction is given by $H = H_0 + H_{QD}$:

$$\begin{aligned}
H_0 = & \sum_{k,\sigma} \epsilon_k a_{k,\sigma}^\dagger a_{k,\sigma} + \sum_{k,\sigma} \epsilon_k b_{k,\sigma}^\dagger b_{k,\sigma} \\
& + \sum_{k,\sigma} V_{k,1} d_{1,\sigma}^\dagger a_{k,\sigma} + \sum_{k,\sigma} V_{k,3} d_{3,\sigma}^\dagger b_{k,\sigma} + c.c
\end{aligned} \tag{1}$$

where the first two terms describe the free electron gas of left and right electrodes. $a_{k,\sigma}^\dagger$ ($b_{k,\sigma}^\dagger$) creates an electron of momentum k and spin σ with energy ϵ_k in the left (right) electrode. $V_{k,\ell}$ ($\ell = 1, 3$) describes the coupling between the electrodes and the first (3-th) QD. $d_{\ell,\sigma}^\dagger$ ($d_{\ell,\sigma}$) creates (destroys) an electron in the ℓ -th dot.

$$\begin{aligned}
H_{QD} = & \sum_{\ell,\sigma} E_\ell n_{\ell,\sigma} + \sum_{\ell} U_\ell n_{\ell,\sigma} n_{\ell,\bar{\sigma}} \\
& + \frac{1}{2} \sum_{\ell,j,\sigma,\sigma'} U_{\ell,j} n_{\ell,\sigma} n_{j,\sigma'} + \sum_{\ell,j,\sigma} t_{\ell,j} d_{\ell,\sigma}^\dagger d_{j,\sigma},
\end{aligned} \tag{2}$$

where E_ℓ is the spin-independent QD energy level, and $n_{\ell,\sigma} = d_{\ell,\sigma}^\dagger d_{\ell,\sigma}$. Notations U_ℓ and $U_{\ell,j}$ describe the intradot and interdot Coulomb interactions, respectively. $t_{\ell,j}$ describes the electron interdot hopping. Here we assume that the interdot hopping and interdot Coulomb interaction in Eq. (2) are appreciable only between the nearest neighbor QDs.

Using the Keldysh-Green's function technique²⁹, the charge current of a TQD junction is calculated according to

$$J = \frac{2e}{h} \int d\epsilon \mathcal{T}(\epsilon) [f_L(\epsilon) - f_R(\epsilon)]. \quad (3)$$

Meanwhile, the heat current that flows into the right (left) electrode from the TQD system is given by

$$Q_{R(L)} = \pm \frac{2}{h} \int d\epsilon \mathcal{T}(\epsilon) (\epsilon - \mu_{R(L)}) [f_L(\epsilon) - f_R(\epsilon)]. \quad (4)$$

We note that $Q_R + Q_L = Q_{Joule} = J\Delta V_a$, which indicates that the heat flux dissipated from the TQD is equal to the electrical power generated by Joule heating.^{23,30} Note that in the open circuit condition ($J = 0$), which is the case for our consideration in the study of electron heat rectification, we have $Q_{Joule} = J\Delta V_a = 0$ and $Q_R = -Q_L$. In Eqs. (3) and (4), $\mathcal{T}(\epsilon) \equiv (\mathcal{T}_{1,3}(\epsilon) + \mathcal{T}_{3,1}(\epsilon))/2$ is the transmission coefficient. $\mathcal{T}_{\ell,j}(\epsilon)$ denotes the transmission function, which can be calculated by using the on-site retarded and lesser Green's functions. The transmission function in the weak interdot hopping limit ($t_{\ell,j} \ll U_\ell$) has the following form,

$$\mathcal{T}_{\ell,j}(\epsilon) = -2 \sum_{m=1}^{32} \frac{\Gamma_\ell(\epsilon) \Gamma_{\ell,j}^m(\epsilon)}{\Gamma_\ell(\epsilon) + \Gamma_{\ell,j}^m(\epsilon)} \text{Im} G_{\ell,m}^r(\epsilon), \quad (5)$$

where "Im" means taking the imaginary part of the function that follows, and

$$G_{\ell,m}^r(\epsilon) = p_{\ell,m} / (\mu_\ell - \Pi_{\ell,m} - \Sigma_{\ell,j}^m), \quad (6)$$

where $\mu_\ell = \epsilon - E_\ell + i\Gamma_\ell/2$. Note that $\Gamma_\ell = 0$ when $\ell \neq 1, 3$. Γ_ℓ denotes the tunneling rate for electron tunneling from QD ℓ to the electrode. In Eqs. (5) and (6), we have $\ell \neq j$. $\Pi_{1(3),m}$ denotes the sum of Coulomb energies between one electron in the first (third) QD and other electrons present in its neighboring QDs in configuration m , and $\Gamma_{\ell,j}^m(\epsilon) = -2\text{Im}\Sigma_{\ell,j}^m(\epsilon)$, where $\Sigma_{\ell,j}^m$ denotes the self energy resulting from electron hopping from QD ℓ to QD j through channel m . The detailed expressions of probability weight $p_{\ell,m}$ as well as $\Pi_{\ell,m}$ and $\Sigma_{\ell,j}^m$ can be found in Ref. 31.

The factor 2 in Eqs. (3) and (4) comes from electron spin degeneracy. $f_{L(R)}(\epsilon) = 1/[e^{(\epsilon - \mu_{L(R)})/k_B T_{L(R)}} + 1]$ denotes the Fermi distribution function for the left (right) electrode.

μ_L and μ_R are the chemical potentials of the left and right leads, respectively, with their average denoted by $E_F = (\mu_L + \mu_R)/2$. $\Delta V_a = (\mu_L - \mu_R)/e$ is the voltage across the TQD junction. $T_{L(R)}$ is the equilibrium temperature of the left (right) electrode. e and h denote the electron charge and Planck's constant, respectively.

To study the LDCT effect on the charge and heat currents of Eqs. (3) and (4), it is important to provide reasonable physical parameters. So far, the exact solution of $\mathcal{T}(\epsilon)$, which are valid for strong-coupling regime (with $t_{\ell,j}$ comparable to $U_{\ell,j}$), has not been reported due to the many body effect.^{8,11} Although the first principles method is often used to calculate $\mathcal{T}(\epsilon)$ directly, it can not handle the charge and heat currents in the Coulomb blockade regime since it is a mean-field approach.²⁵ Here, we use the extended Hubbard-Anderson model ($H = H_0 + H_{QD}$) to illustrate the transport and thermoelectric properties of three disk-like (or cone-shaped) GaAs QDs embedded in $\text{Al}_x\text{Ga}_{1-x}\text{As}$ connected to electrodes. The physical parameters for $U_{\ell,j}$ and $t_{\ell,j}$ used in H_{QD} can be calculated in the framework of effective mass method.³² The effective-mass equation for a coupled QD (CQD) system is given by

$$[-\nabla \frac{\hbar^2}{2m^*(\rho, z)} \nabla + V_{CQD}(\rho, z) + V_{sc}(\mathbf{r})]\psi(\mathbf{r}) = E\psi(\mathbf{r}), \quad (7)$$

where $m_e^*(\rho, z)$ denotes the position-dependent electron effective mass. We adopt effective masses $m_{GaAs}^* = 0.063 m_e$ for GaAs and $m^* = 0.096 m_e$ for $\text{Al}_{0.4}\text{Ga}_{0.6}\text{As}$. $V_{CQD}(\rho, z)$ is approximated by a constant potential $V_0 = -0.2496 \text{ eV}$ in the QD region and zero in the barrier region. Its value is determined by the conduction band offset between GaAs and $\text{Al}_{0.4}\text{Ga}_{0.6}\text{As}$. $V_{sc}(\mathbf{r}) = \frac{e^2}{\epsilon_0} \int d\mathbf{r}' n_e(\mathbf{r}')/|\mathbf{r} - \mathbf{r}'|$ denotes the self-consistent potential caused by the electrostatic interaction with the charge density associated with the other particles in the system. Note that we consider the position-independent dielectric constant $\epsilon_0 = 15.5$. For the purpose of constructing approximate wave functions, we place the system in a large cylindrical confining box with the length L and radius R (L and R must be much larger than those of CQD). Here we choose $L = 60 \text{ nm}$ and $R = 40 \text{ nm}$. We solve Eq. (7) by the Ritz variational method.³² The wave functions are expanded in a set of basis functions, which are chosen to be products of Bessel functions of ρ and sine functions of z ,

$$\psi_{n,\ell,m}(\rho, z, \phi) = J_\ell(\beta_n \rho) e^{i\ell\phi} \sin(k_m(z + L/2)), \quad (8)$$

where $k_m = m\pi/L$, $m = 1, 2, 3, \dots$, J_ℓ is the Bessel function of order ℓ and $\beta_n R$ is the n th zero of J_ℓ . The expression of the matrix elements of Eq. (7) can be readily obtained. Forty-five

sine functions multiplied by fifteen Bessel functions for each angular function ($\ell = 0$ or 1) are used to diagonalize H_{CQD} . A convergence check (by increasing the basis functions) indicates that the lowest two confined states are accurate to within 0.1 meV with the current set of bases.

Figure 1 shows (a) energy levels and (b) electron hopping strengths for two different shapes of GaAs QDs (cone and disk) as functions of the gap distance (D) between two QDs. The height and radius of each QD are $L_1 = L_2 = 5 \text{ nm}$ and $R_1 = R_2 = 10 \text{ nm}$. Let t_c denotes the hopping strength between adjacent QDs in a tight-binding model. The energy separation between the bonding ($E_{BD} = E_0 + t_c$) and antibonding ($E_{AB} = E_0 - t_c$) states increases with decreasing gap distance (D). The electron hopping strength ($t_{\ell,j} = t_c$) is smaller than 0.1 meV when the gap distance D is larger than 10 nm . When $D = 4 \text{ nm}$, t_c is approximately 3.5 meV . Note that $t_{\ell,j}$ as a function of gap distance can be fitted very well by an exponential decay function, which can be used to estimate the very weak coupling for two QDs separated far away. As seen in Fig. 1(b), when the gap distance is doubled, $t_{\ell,j}$ reduces to 0.36 meV (a factor 10 smaller). Therefore, it is adequate to keep the inter-dot coupling $t_{\ell,j}$ only for adjacent dots, since $t_{1,3}$ (between two outer dots) is significantly smaller. To evaluate the electron Coulomb interaction strengths, we calculate the intradot and interdot Coulomb interactions as functions of the gap distance (D) for two disk-shaped QDs: dot A with $L_1 = 5 \text{ nm}$ and $R_1 = 10 \text{ nm}$ and dot B with $L_2 = 5.5 \text{ nm}$ and $R_2 = 11 \text{ nm}$. The results are shown in Fig. 1(c). The position dependence for intradot Coulomb interactions are noticeable only for small D , where the leak-out of QD wave function is appreciable.

In the presence of an applied bias, the resulting electric field leads to the energy level shift. To examine this effect, we added a term $-eF(z - z_0)$ in Eq. (7). F and z_0 denote the electric-field strength and the middle point of the junction, respectively. Figure 2 shows the lowest two energy levels as functions of electric-field strength (F) for disk-shaped QDs with (a) identical QD sizes ($R_1 = R_2 = 10 \text{ nm}$) and (b) different QD sizes ($R_1 = 10 \text{ nm}$ and $R_2 = 9 \text{ nm}$), while $L_1 = L_2 = 5 \text{ nm}$. In Fig. 2(a), the energy gap ($2t_c$) arises from the resonant tunneling between E_1 and E_2 levels in the absence of F . When F increases, this resonant coupling is diminished (off resonance) due to the increased separation of E_1 and E_2 , which is approximately linear in F . In Fig. 2(b), E_1 and E_2 levels are "off resonance" in the absence of F . However, F can be tuned to bring the E_1 and E_2 levels in resonance [see Fig. 2(b) near $F = 3 \text{ kV/cm}$]. The results of Fig. 2 indicate that the energy level shift

as well as $t_{\ell,j}$ and $U_{\ell}(U_{\ell,j})$ will significantly affect the behaviors of charge and heat currents.

For electrodes made of heavy-doped semiconductors, the Fermi energy of semiconductor electrode depends on the carrier concentration. For example, the carrier concentration $n = 2 \times 10^{18}/\text{cm}^3$ in the *GaAs* electrodes leads to $E_F = 91.76 \text{ meV}$. Therefore, we have $E_{\ell} - E_F = 7.24 \text{ meV}$ for disk-shaped QDs described by the solid lines in Fig. 1(a). The level $E_{\ell} - E_F$ can be tuned by a gate electrode or the carrier concentration of electrodes. In the following numerical calculations, we consider a GaAs/AlGaAs TQD junction with gap distance $D = 8 \text{ nm}$ and QD size $L_{\ell} = 5 \text{ nm}$. Using the effective-mass model described above, we obtain $U_{\ell} = 200\Gamma_0$, $U_{\ell,j} = 66\Gamma_0$, and $t_{\ell,j} = 3.6\Gamma_0$, where $\Gamma_0 = 0.1 \text{ meV}$. This set of physical parameters satisfies the condition of $U_{\ell} > U_{\ell,j} \gg t_{\ell,j}$ and $U_{\ell} \gg \Gamma_{\ell}$, which are required in keeping the validity of Eq. (5) for $\mathcal{T}(\epsilon)$.³¹ The tunneling rates Γ_{ℓ} can also be accurately determined by a stabilization method.³²

III. RESULTS AND DISCUSSION

A. LDCT for charge current

The results of Fig. 2 show that the bias-dependent shift of energy level (E_{ℓ}) in each dot can be approximately determined according to the expression $\epsilon_{\ell} = E_{\ell} + \eta_{\ell}e\Delta V_a$, where η_{ℓ} denotes the fraction of voltage difference shared by QD ℓ . The value of η_{ℓ} depends on the location, shape and dielectric constant of the QD. When the dielectric constants of the QD and the surrounding material are similar, the voltage difference is almost uniformly distributed among QDs. Let d_{ℓ} denotes the center position of QD ℓ with respect to the mid point of the junction and the separation of two electrodes is D_{LR} , then the electrostatic potential energy due to the uniform electric field seen by an electron in QD ℓ is simply $V(\mathbf{r} - d_{\ell}\hat{z}) = [d_{\ell} + (z - d_{\ell})](-e\Delta V_a/D_{LR})$ (z is along the direction of transport). For weak field and symmetric wave function in each QD, the linear $(z - d_{\ell})$ term vanishes, and the energy correction due to second-order Stark effect is insignificant. Thus, we have $\eta_{\ell} = d_{\ell}/D_{LR}$. For the TQD junction, we assume $d_1 = -d_3$ and $\eta_1 = -\eta_3$.

We first calculate the tunneling current for $\Gamma_L = \Gamma_R \equiv \Gamma$ (with $\Gamma = 0.3\Gamma_0$) under thermal equilibrium. Figure 3(a) shows the tunneling current as a function of the applied bias ΔV_a for a GaAs/AlGaAs TQD junction with staircase energy levels ($E_1 = E_F + 9\Gamma_0$,

$E_2 = E_F + 6\Gamma_0$ and $E_3 = E_F + 3\Gamma_0$), $\eta_1 = -\eta_3 = 0.24$, and $D_{LR} = 54 \text{ nm}$. Such an energy level arrangement was also considered in Ref. 6. We noticed a negative differential conductance (NDC) behavior. This is an essential feature for resonant tunneling junction due to off-resonance process.⁴⁻⁶ There is an unexpected resonance peak at $\Delta V_a = 125\Gamma_0$ labeled by p_3 , whose contribution is mainly from the 3rd configuration as described in Ref. 31. This p_3 resonance peak can be suppressed by decreasing temperature. The structure labeled by p_3 arises from the LDCT between the outer QDs associated with charging effect under the resonant condition with energy levels $\epsilon_1 \equiv E_1 + 0.24e\Delta V_a = E_3 + U_{23} - 0.24e\Delta V_a \equiv \epsilon_3$. Note that $\epsilon_2 \equiv E_2 + U_{23}$ and E_2 do not have to be resonant with $\epsilon_1 = \epsilon_3$, a main feature of LDCT. The p_3 structure indicates that the middle QD can assist the electron tunneling between outer QDs separated by a large distance through a new channel in the presence of electron Coulomb interaction. In the p_3 configuration, there is one electron in level E_3 with the same spin σ as the electron entering the junction from the electrode [see the inset of Fig. 3(a)]. Lowering the temperature decreases the probability of electron occupation in level E_3 (N_3). Therefore, the peak of p_3 decreases with decreasing temperature. It is noted that even at extremely low temperature, a residue value of N_3 still exists. The tiny structure labeled by p_3 at very low temperature can be resolved in the differential conductance.

In order to illustrate the effect of electron Coulomb interactions, we also show in Fig. 3(a) the tunneling current at $k_B T = 6\Gamma_0$ (curve with triangle marks) for the case without Coulomb interactions (i.e. $U_\ell = U_{\ell,j} = 0$). In this case, the structure labeled by p_3 vanishes, whereas the magnitude of J is enhanced. We note that Fig. 3(a) displays a nearly temperature-independent thermal broadening effect, which is very different from that of a single QD junction.^{13,14} Such a "nonthermal" broadening effect is a common feature for serially double QD junction system.^{15,33} Reference 33 pointed out that such a "nonthermal" broadening effect allows serially double QDs to function as low-temperature filters. The detailed description of low-temperature filter can be found in Ref. 33, where the electron Coulomb interactions were neglected.

Because it is difficult to get an analytic expression of tunneling current shown in Fig. 3(a), we illustrate the effect of LDCT on the electrical conductance of the TQD junction, where the QD levels are aligned with E_F . For this case, simple expressions can be used to reveal the LDCT effect. We show in Fig. 3(b) the electrical conductance (G_e) as a function of gate

voltage V_g , which is applied to tune the middle-dot level, E_2 . Note that

$$G_e = \frac{2e^2}{h} \int d\epsilon \mathcal{T}(\epsilon) \left(-\frac{\partial f}{\partial \epsilon}\right). \quad (9)$$

Here, $E_1 = E_3 = E_F$ and $E_2 + eV_g = E_F + eV_g$. The trend of G_e with respect to eV_g can be well explained by Eq. (3) with transmission coefficient $\mathcal{T}(\epsilon) \approx \mathcal{T}^1(\epsilon) = (\mathcal{T}_{1,3}^1(\epsilon) + \mathcal{T}_{3,1}^1(\epsilon))/2$.

$$\mathcal{T}^1(\epsilon) = \frac{\Gamma_L \Gamma_R t_{eff}^2(\epsilon) p_1}{|\mu_1 \mu_3 - t_{eff}(\epsilon) \mu_3 - t_{eff}(\epsilon) \mu_1|^2}, \quad (10)$$

where $\mu_1 = \epsilon - E_1 + i\Gamma/2$ and $\mu_3 = \epsilon - E_3 + i\Gamma/2$. $t_{eff}(\epsilon) = t_c^2/(\epsilon - E_2 - eV_g)$.

In the absence of U_ℓ and $U_{\ell,j}$, a similar expression to Eq. (10) can also be found in Ref. 34. The authors of Ref. 34 considered the effect of electron Coulomb interactions within the Hartree-Fock approximation. With this approximation, the electron occupation numbers will appear in the denominator of Eq. (10). This will lead to a fractional charge picture. In our procedure used for calculating the retarded and lesser Green functions (which is beyond the Hartree-Fock approximation), the electron occupation numbers and two-particle correlation functions appear only in the probability weight of each configuration.^{31,35} The picture with integer charges appearing in the denominators of Eq. (6) is consistent with that of the master equation method.¹¹ In this approach, we only considered the one-particle occupation number and on-site two particle correlation functions in the probability weights. For weak interdot hopping strength ($t_{\ell,j}/\Gamma < 1$), the approximation which neglects the two-particle interdot correlation functions and higher order functions can get results quite close to those obtained by solving the equation of motion exactly (i.e. including all correlation functions) via numerical computation, which has been done and will be reported elsewhere.³⁶ Although such an approximation is not so accurate for $t_{\ell,j}/\Gamma > 1$ when QD energy levels are degenerate, the procedure considered in Eq. (5)^{16,31} is justified as long as $|E_\ell - E_j|/t_{\ell,j} \gg 1$.

We note that $\mathcal{T}(\epsilon)$ is equal to $\mathcal{T}^1(\epsilon)$ with $p_1 = 1$ in the absence of electron Coulomb interactions.³¹ With finite electron Coulomb interactions we have $p_1 = (1 - N_1)(1 - 2N_2 + c_2)(1 - 2N_3 + c_3)$, where N_ℓ is the one-electron occupancy in E_ℓ level. Note that $N_1 = N_3$ for the symmetrical configuration shown in the inset of Fig. 3(b). The probability of two-electron occupancy c_ℓ in each QD can be assumed zero due to the large value of U_ℓ . The curve with triangle marks in Fig. 3(b) shows G_e in the absence of electron Coulomb interactions at $k_B T = 3\Gamma_0$. We find that G_e increases initially, reaching a maximum, then decreases as V_g increases. When the electron Coulomb interactions are included, the probability factor

p_1 becomes V_g dependent (as shown in the curve with squares), which modifies the behavior of G_e as shown in the solid, dashed, and dotted curves at $k_B T = 1, 2$, and $3\Gamma_0$.

Based on Eq. (10), the solution of G_e might be expressed in terms of the poly-Gamma functions.³³ Rather than using the complicate poly-Gamma functions, we derive some simple expressions from Eq. (10) in suitable limits to gain better understanding of the behavior of G_e . In the linear response regime with respect to ΔV_a , the energy levels shifted by ΔV_a can be neglected in Eq. (10). Since $E_1 = E_3 = E_F$ here, Eq. (10) reduces to $\mathcal{T}^1(\epsilon) = \frac{p_1 \Gamma_L \Gamma_R t_c^4}{|\mu_1(\mu_1(\epsilon - E_2 - eV_g) - 2t_c^2)|^2}$. The denominator can be rewritten in the form $|(\epsilon - E_F + i\Gamma/2)(\epsilon - \tilde{\epsilon}_+)(\epsilon - \tilde{\epsilon}_-)|^2$, where

$$\tilde{\epsilon}_{\pm} = E_F - i\Gamma/2 + [(eV_g + i\Gamma/2) \pm \sqrt{(eV_g + i\Gamma/2)^2 + 8t_c^2}]/2 \quad (11)$$

denote the energy positions of two poles in addition to the pole at $E_F - i\Gamma/2$. At $V_g = 0$, the two poles $\tilde{\epsilon}_{\pm} = E_F - i\Gamma/4 \pm \sqrt{2}t_c$ when $t_c \gg \Gamma$, which are located far from E_F (since $t_c \gg \Gamma$) and their contributions to G_e become negligible. Thus, at $V_g = 0$ we have

$$G_e \approx \frac{e^2}{h} \frac{p_1 \pi \Gamma}{2k_B T}, \quad (12)$$

which is dominated by the pole at $\epsilon = E_F$. However, when V_g increases, the two poles at $\tilde{\epsilon}_{\pm}$ move up in energy [See Eq. (11)] with the lower pole approaching the level E_F , which gives appreciable contribution to G_e when the pole is in the range covered by the function $(-\frac{\partial f}{\partial \epsilon}) = 1/[4k_B T \cosh^2(\frac{\epsilon - E_F}{2k_B T})]$ appearing in Eq. (9). This explains the initial rise of G_e (for $p_1 = 1$) with respect to V_g at finite temperatures as seen in Fig. 3(b). As temperature approaches zero, the function $(-\frac{\partial f}{\partial \epsilon})$ turns into a delta function with $\epsilon = E_F$, then we have $G_e = \frac{2e^2}{h} \mathcal{T}(E_F) \approx (2e^2/h)p_1/[1 + (eV_g \Gamma/(4t_c^2))^2]$. Thus, at $T = 0$, the maximum of G_e would occur at $V_g = 0$.

To understand the decrease of G_e for large values of V_g we consider another asymptotic expression (for $k_B T > \Gamma > t_{eff}$)

$$G_e \approx \frac{e^2}{h} \frac{\pi \Gamma}{2k_B T} \frac{p_1 t_{eff}^2}{t_{eff}^2 + \Gamma^2/4}, \quad (13)$$

where $t_{eff} = t_c^2/(eV_g)$. As V_g approaches infinity, we obtain an insulating state ($G_e \rightarrow 0$).

The curves with circle marks are calculated by Eq. (13) for the case including Coulomb interactions at $k_B T = 1\Gamma_0$ and excluding Coulomb interactions at $k_B T = 3\Gamma_0$ (i.e. $p_1 = 1$). We find good agreement between results obtained by Eq. (10) and by the asymptotic

expression (13) for $eV_g > 43\Gamma_0$. The factor $k_B T$ appearing in the denominator of Eqs. (12) and (13) also explains why G_e is suppressed with increasing temperature, as seen in Fig. 3(b). The simple expression of Eq. (13) is the manifestation of the result for a DQD with effective coupling strength t_{eff} .³³ It is convenient to use Eq. (13) to illustrate the effect of LDCT between the outer QDs separated by a large distance.

For $t_c = 0.36 \text{ meV}$ (with $D = 8 \text{ nm}$ between the middle QD and the outer QD), we obtain $t_{eff} = 25.9 \text{ } \mu\text{eV}$ for $eV_g = 5 \text{ meV}$ between outer QDs separated by barriers with total thickness $D = 16 \text{ nm}$. (Note: the width of the middle QD does not count toward the gap distance. Only the barrier thickness counts) For such a gap distance, the direct coupling for outer GaAs/GaAlAs QDs is $t_{13} = 1.73 \mu\text{eV}$, which is negligible compared to t_{eff} . The effect of LDCT is very useful for improving the entanglement between qubits stored in distant QDs.^{4,5} Next, we investigate how LDCT influences the electron heat rectification of TQD junctions.

B. LDCT for heat current

To study the direction-dependent heat current, we let $T_L = T_0 + \Delta T/2$ and $T_R = T_0 - \Delta T/2$, where $T_0 = (T_L + T_R)/2$ is the average of equilibrium temperatures of two side electrodes and $\Delta T = T_L - T_R$ is the temperature difference across the junction. We have numerically solved Eqs. (3) and (4) for TQD junctions. We first determine the nonlinear Seebeck coefficient $S = e\Delta V_{th}/k_B \Delta T$ (thermal voltage yielded by ΔT) by solving Eq. (3) with $J = 0$ (the open circuit condition) for a given ΔT , T_0 and an initial guess of the average one-particle and two-particle occupancy numbers, N and c for each QD, which can be found in Ref. 31. Due to $J = 0$, we have $Q_{Joule} = 0$. Once ΔV_{th} is solved, we then use Eq. (4) to compute the heat current. The nonlinear Seebeck coefficient of a single molecule was studied in references [25,26] for the applications of thermal spintronics. Fig. 4(a) shows the electron heat current ($Q = Q_R$) as a function of temperature bias ΔT for various values of energy alignment $\Delta_F = E_3 - E_F$ (while keeping $E_1 = E_3 + 2\Delta_0$, and $E_2 = E_3 + \Delta_0$) at $T_0 = 26\Gamma_0$, and $\Gamma_L = \Gamma_R = 7\Gamma_0$. Note that $D_{LR} = 43 \text{ nm}$, we have $\eta_1 = -\eta_3 = 0.31$. The energy levels of the TQD have a staircase structure with step height $\Delta_0 = 20\Gamma_0$. We considered $\Delta_0 = 20\Gamma_0$, which is larger than that considered in Fig. 3, for observing electron heat rectification in a wide temperature range. The results of Fig. 4(a) indicate an asymmetrical

heat current (rectification effect) which depends on Δ_F . When T_0 is larger than Δ_F , the rectification effect is seriously suppressed. The dash-dotted line is almost symmetric, which means Q is linearly proportional to ΔT .

To further enhance the asymmetrical behavior, we study the heat current (Q) for various values of T_0 at $\Delta_F = 40\Gamma_0$ as shown in Fig. 4(b). Other physical parameters are the same as those for the solid line in Fig. 4(a). When the averaged temperature T_0 goes down, the forward heat current (Q_F) increases in the forward temperature bias ($\Delta T > 0$), whereas the backward heat current (Q_B) decreases in the reversed temperature bias ($\Delta T < 0$). The asymmetrical Q behavior with respect to ΔT is enhanced with decreasing T_0 . Because QD energy levels are shifted by the thermal voltage (ΔV_{th}), we show in Fig. 4(c) and 4(d) the thermal voltage ΔV_{th} yielded by ΔT , corresponding to Fig. 4(a) and 4(b), respectively. As shown in Fig. 4(c), when $\Delta_F = 10\Gamma_0$ the thermal voltage ΔV_{th} produced is rather small, which is insufficient to give rise to noticeable nonlinear heat behavior with respect to ΔT [See dash-dotted line in Fig. 4(a)]. Figure 4(d) shows the increase of nonlinear behavior in Q due to the enhancement of ΔV_{th} . In addition, the results of Fig. 4 also indicate that there exists a nonlinear relationship between Q and ΔV_{th} . The results of Fig. 4(b) (large heat current in $\Delta T > 0$ and small heat current in $\Delta T < 0$) can be understood by the following. The transmission coefficient $\mathcal{T}_{\ell,j}^m(\epsilon)$ of the dominant configuration is proportional to the joint density of states (JDOS), which is the product of spectral functions arising from three resonant poles (see Eq. (7) of Ref. 31). The thermal voltage ΔV_{th} causes shift in the QD levels. Thus, for a TQD system with $E_1 > E_2 > E_3$ under zero bias (see the inset of Fig. 4(c)), a positive ΔT can bring the levels close to resonance, while a negative ΔT will cause them further apart from resonance, resulting a increases (decreases) in JDOS when $\Delta T > 0$ ($\Delta T < 0$).

Next, we examine the LDCT effect on the rectification behavior of the TQD junction. Figure 5 shows the heat current and thermal voltage as functions of temperature bias for $\Delta_F = E_3 - E_F = 40\Gamma_0$ and $E_1 = E_3 + 25\Gamma_0$ for various values of E_2 . As E_2 increases from $E_3 + 12.5\Gamma_0$ to $E_3 + 25\Gamma_0$, the thermal voltage ΔV_{th} increases. In comparison to the results of Figs. 4(b), the heat current of forward temperature bias in Fig. 5 is enhanced significantly, which is attributed to the enhancement of JDOS resulting from the better alignment of resonant poles. For the forward temperature bias ($\Delta T = 12.5\Gamma_0$), the energy levels of outer QDs can be aligned at $\Delta V_{th} = -40.3\Gamma_0$ (LDCT resonant level $E_{LDCT} = E_F + 52.5\Gamma_0$), while

the middle QD energy level is misaligned with E_{LDCT} , which leads to an effective tunneling coupling $t_{eff} = t_c^2/(E_2 - E_{LDCT})$. From the results of Fig. 5, we see that the LDCT can also improve the heat rectification behavior for two distant QDs.²⁸ To observe such an electron heat rectification effect shown in Fig. 4(b) and 5, the magnitude of phonon heat current Q_{ph} must not be dominant over the electron heat current. To reduce Q_{ph} , we can design a QD array in which the barriers (AlGaAs) have a small cross section (see the inset of Fig. 5(a)) to produce a phonon bottleneck effect.²⁸ Although many studies have been devoted to the design of phonon or photon heat rectifiers,^{37–39} these designs are not compatible with the fabrication technique of solid state quantum register circuit. So far, few experiments have observed the heat rectification effect.⁴⁰

IV. SUMMARY

We have theoretically studied the effect of LDCT on the charge and heat currents of a TQD junction in the Coulomb blockade regime. In the presence of intradot and interdot Coulomb interactions the closed form Landauer expression for transmission coefficient provides a useful analysis for clarifying the influence of electron Coulomb interactions on the LDCT effect. The middle QD can mediate the coherent tunneling between distant outer QDs. An interesting electron heat rectification effect of the TQD junction is demonstrated by considering a staircase-like alignment of energy levels. Using the nonlinear Seebeck effect ($e\Delta V_{th}/k_B\Delta T$), we can control the electron resonant process of the TQD junction by temperature bias to observe heat rectification.

Acknowledgments

This work was supported in part by the National Science Council of the Republic of China under Contract Nos. NSC 101-2112-M-008-014-MY2, and NSC 101-2112-M-001-024-MY3.

E-mail address: mtkuo@ee.ncu.edu.tw

E-mail address: yiachang@gate.sinica.edu.tw

-
- ¹ D. Loss and D. P. DiVincenzo, Phys. Rev. A **47**, 120 (1998).
 - ² R. Hanson, L. P. Kouwenhoven, J. R. Petta, S. Tarucha, and L. M. K. Vandersypen, Rev. Mod. Phys. **79**, 1217 (2007).
 - ³ K. Ono, D. G. Austing, Y. Tokura, S. Tarucha, *Science* **297**, 1313 (2002).
 - ⁹ M. Busl, G. Granger, L. Gradreau, R. Sanchez, A. Kam, M. Pioro-Ladriers, S. A. Studenikin, P. Zawadzki, Z. R. Wasilewski, A. S. Sachrajda and G. Platero, Nature Nanotech **8**, 261 (2013).
 - ⁵ F. R. Braakman, P. Barthelemy, C. Reichi, W. Wegscheider, and L. M. K. Vandersypen, Nature Nanotech **8**, 432 (2013).
 - ⁶ S. Amaha, W. Izumida, S. Teraoka, S. Tarucha, J. A. Gupta and D. G. Austing, Phys. Rev. Lett. **110**, 016803 (2013).
 - ⁷ W. A. Harrison, Applied Quantum Mechaics, (World scientific, Singapore, 2000)
 - ⁸ M. Korkusinski, I. P. Gimenez, P. Hawrylak, L. Gaudreaus, S. A. Studenikin, and A. S. Sachrajda, Phys. Rev. B **75**, 115301 (2007).
 - ⁹ M. Busl, R. Sanchez, and G. Platero, Phys. Rev. B **81**, 121306 (2010).
 - ¹⁰ I. Weymann, B. R. Bulka, and J. Barnas, Phys. Rev. B **83**, 195302 (2011).
 - ¹¹ C. Y. Hsieh, Y. P. Shim and P. Hawrylak, Phys. Rev. B **85**, 085309 (2012).
 - ¹² M. Zebarjadi, K. Esfarjania, M.S. Dresselhaus, Z.F. Ren and G. Chen, Energy Environ Sci **5**, 5147 (2012).
 - ¹³ P. Murphy, S. Mukerjee, and J. Moore, Phys. Rev. B **78**, 161406 (2008).
 - ¹⁴ D. M. T. Kuo and Y. C. Chang, Phys. Rev. B **81**, 205321 (2010).
 - ¹⁵ D. M. T. Kuo, S. Y. Shiau and Y. C. Chang, Phys. Rev. B **84**, 245303 (2011).
 - ¹⁶ D. M. T. Kuo and Y. C. Chang, Nanoscale Res. Lett. **7**, 257 (2012).
 - ¹⁷ D. M. T. Kuo and Y. C. Chang, Nanotechnology **24**, 175403 (2013).
 - ¹⁸ Q. Wang, H. Xie, Y. H. Nie and W. Ren, Phys. Rev. B **87**, 075102 (2013).
 - ¹⁹ D. Segal, Phys. Rev. Lett. **100**, 105901 (2008).
 - ²⁰ B. Sothmann, R. Sanchez, A. N. Jordan and M. Buttiker, Phys. Rev. B **85**, 205301 (2012).
 - ²¹ R. S. Whitney, Phys. Rev. B **87**, 115404 (2013).
 - ²² S. Juergens, F. Haupt, M. Moskalets, and J. Splettstoesser, Phys. Rev. B **87**, 245423 (2013)

- ²³ R. Lopez and D. Sanchez, Phys. Rev. B **88**, 045129 (2013).
- ²⁴ J. Meair and P. Jacquod, J. Phys.: Condens. Matter **25**, 082201 (2013).
- ²⁵ Y. S. Liu and Y. C. Chen, Phys. Rev. B **79**, 193101 (2009)
- ²⁶ J. Fransson and M. Galperin, Phys. Chem. Chem. Phys. **13**, 14350 (2011).
- ²⁷ D. Sanchez and R. Lopez, Phys. Rev. Lett. **110**, 026804 (2013).
- ²⁸ Y. C. Tseng, D. M. T. Kuo, Y. C. Chang and Y. T. Lin, Appl. Phys. Lett. **103**, 053108 (2013).
- ²⁹ H. Haug and A. P. Jauho, Quantum Kinetics in Transport and Optics of Semiconductors (Springer, Heidelberg, 1996).
- ³⁰ A. Crepieux and F. Michelini, Int. J. Nanotechnol, **9** 355 (2012).
- ³¹ D. M. T. Kuo and Y. C. Chang, arXiv:1209.0506.v3
- ³² D. M. T. Kuo and Y. C. Chang, Phys. Rev. B **61**, 11051 (2000).
- ³³ L. Oroszlany, A. Kormanyos, J. Koltai, J. Cserti and C. J. Lambert, Phys. Rev. B **76**, 045318 (2007).
- ³⁴ Y. Liu, Y. Zheng, W. Gong, W. Cao and T. Lu, Phys. Lett. A **365**, 495 (2007).
- ³⁵ B. R. Bulka and T. Kostyrko, Phys. Rev. B **70**, 205333 (2004).
- ³⁶ C. C. Chen, Y. C. Chang, and D. M. T. Kuo, unpublished.
- ³⁷ B. Li, L. Wang and G. Casati, Phys. Rev. Lett. **93** 184301 (2004).
- ³⁸ B. B. Hu, L. Yang, and Y. Zhang Phys. Rev. Lett. **97** 124302 (2006).
- ³⁹ C. R. Otey, W. T. Lau, and S. H. Fan, Phys. Rev. Lett. **104** 154301 (2010).
- ⁴⁰ C. W. Chang, D. Okawa¹, A. Majumdar, and A. Zettl, Science **17** 1121 (2006).

Figure captions

Fig. 1. (a) Energy levels and (b) electron hopping strength of identical double quantum dots (GaAs/AlGaAs) as a function of gap distance (D). (c) Intradot and interdot Coulomb interactions as a function of D for Dot A and dot B with, respectively, the height $L_1 = 5nm$ (radius $R_1 = 2L_1$) and $L_2 = 5.5 nm$ (radius $R_2 = 2L_2$).

Fig. 2. The lowest two energy levels of coupled QDs as a function of electric field strength (F) for two different gap distances. (a) Identical QD sizes, and (b) different QD sizes. The other physical parameters are the same as those for solid lines of Fig. 1(a).

Fig. 3. (a) Tunneling current as a function of applied bias ΔV_a for the variation of temperatures, and (b) electrical conductance (G_e) as a function of $E_2 - E_F = eV_g$ for various temperatures with $E_1 = E_3 = E_F$. In diagram (a) we have $\epsilon_2 = E_2 + U_{23}$, $\epsilon_3 = E_3 + U_{23}$, and $J_0 = 2e\Gamma_0/h$.

Fig. 4. (a) Electron heat current ($Q = Q_R$) as a function of temperature bias ΔT for TQD junction with staircase energy levels at $k_B T_0 = 26\Gamma_0$ and $D = 8 nm$. (b) Q for different T_0 values. Other physical parameters are the same as those for the solid line in (a). (c) and (d) are the thermal voltage (ΔV_{th}) corresponding to (a) and (b), respectively. $Q_0 = \Gamma_0^2/h$.

Fig. 5: (a) Heat current (Q), and (b) thermal voltage ($e\Delta V_{th}$) as a function of temperature bias for different values of E_2 at $E_1 = E_3 + 25\Gamma_0$ and $E_3 = E_F + 40\Gamma_0$. Other physical parameters are the same as those of dash-dotted line in Fig. 4(b).

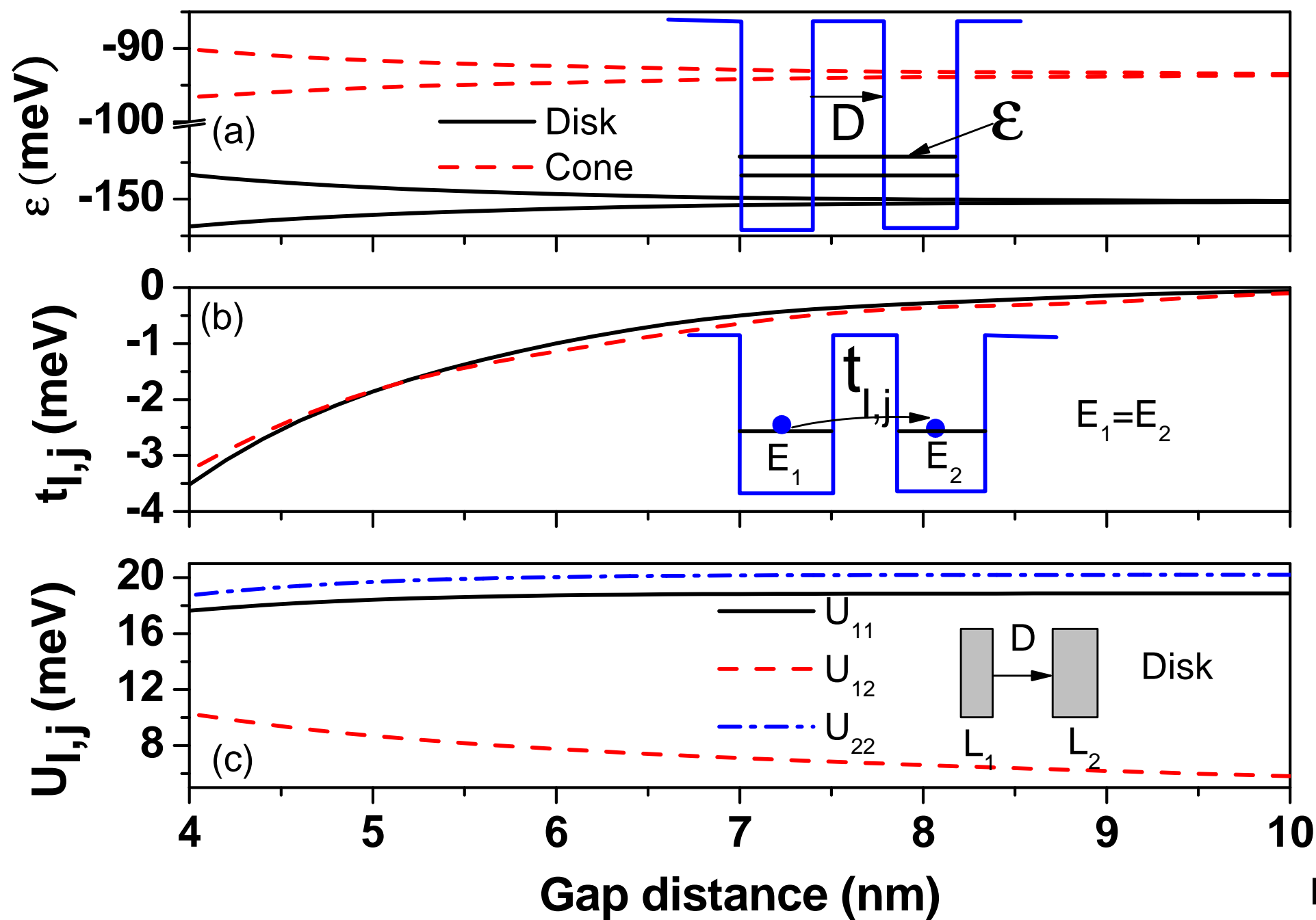


Fig1

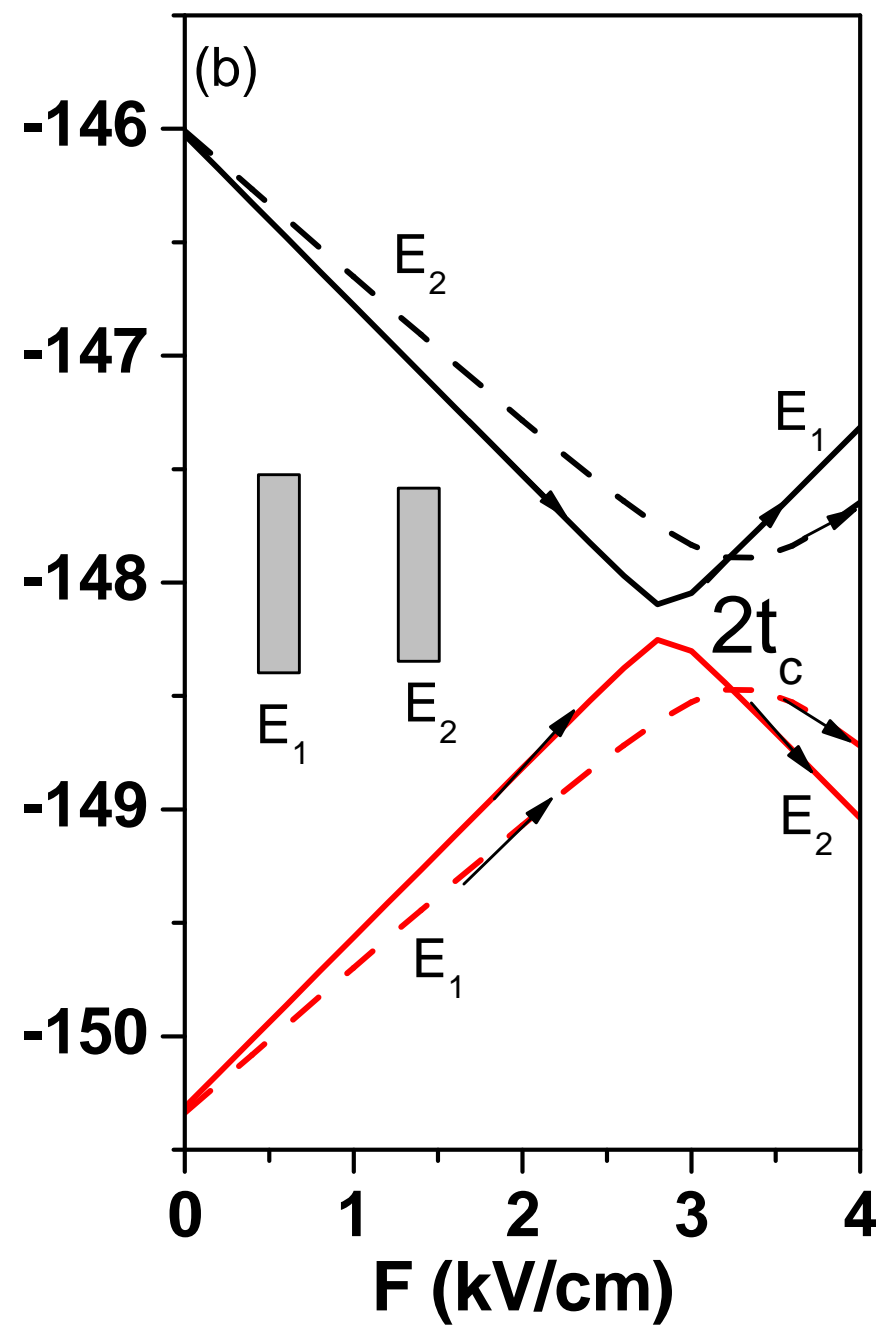
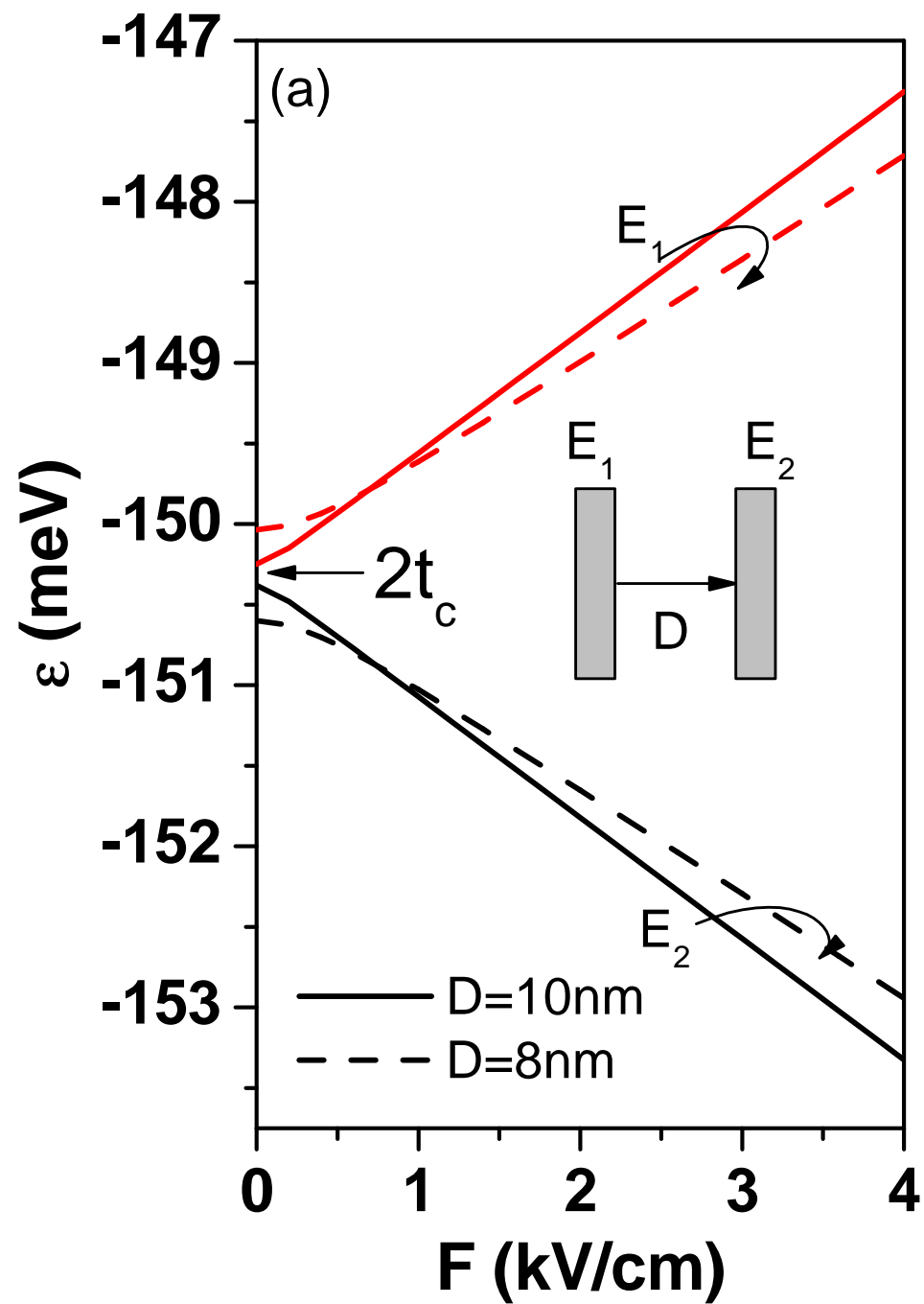


Fig2

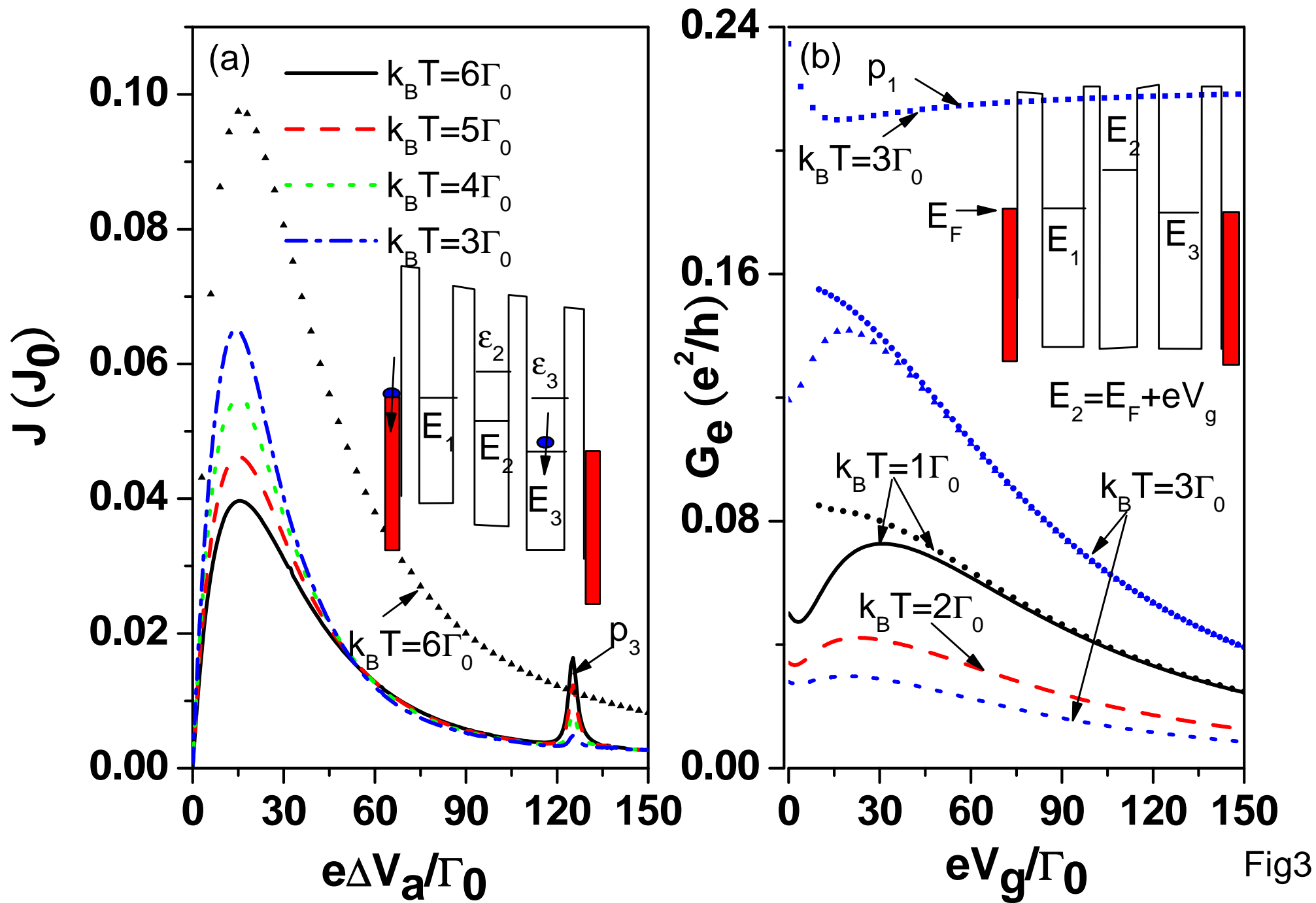


Fig3

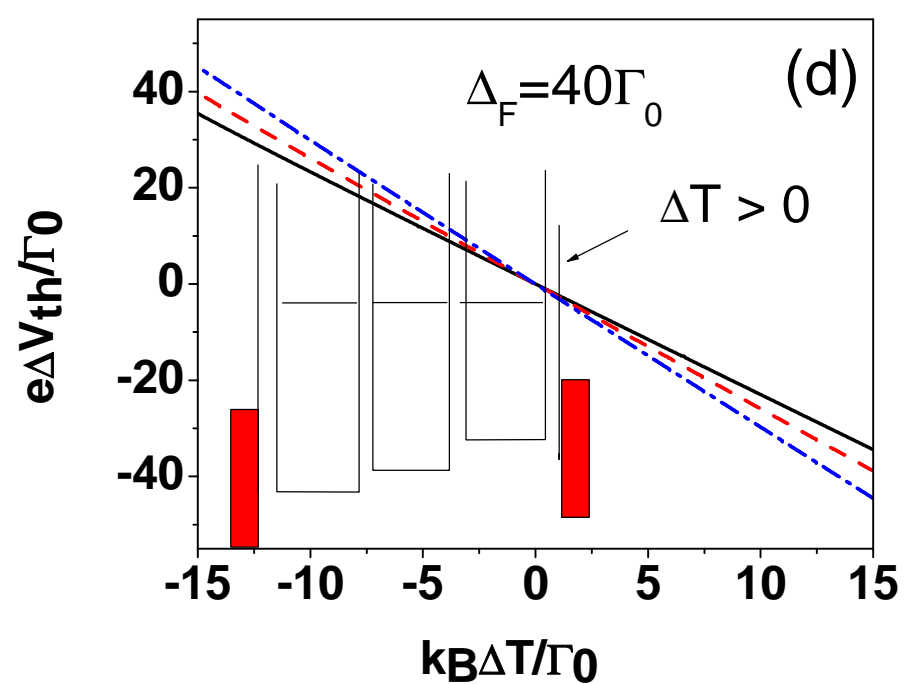
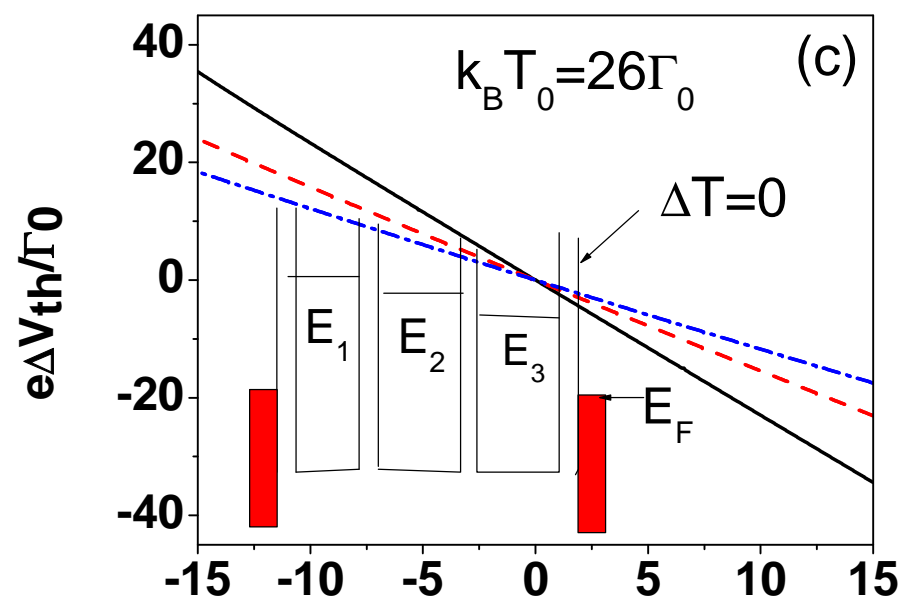
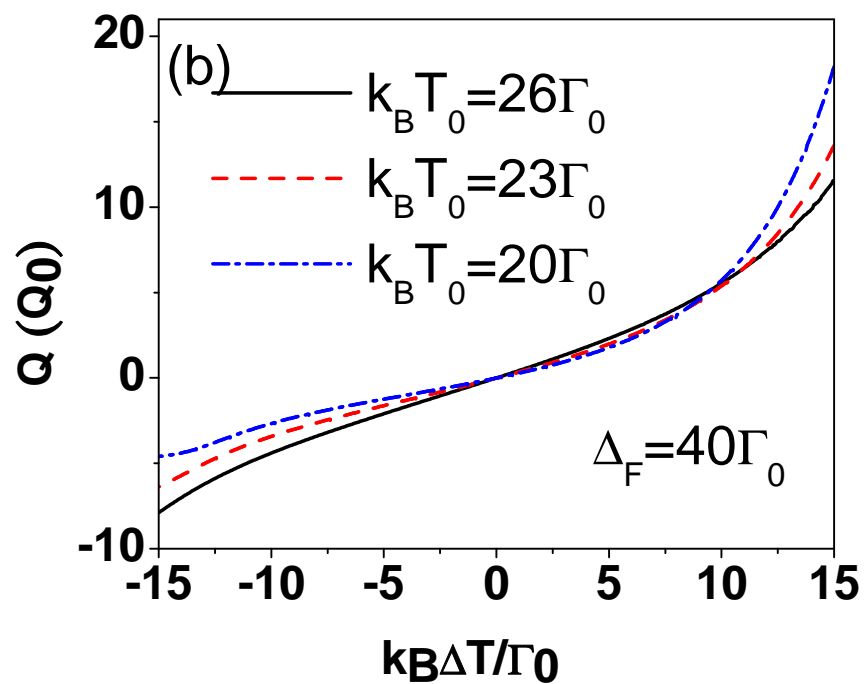
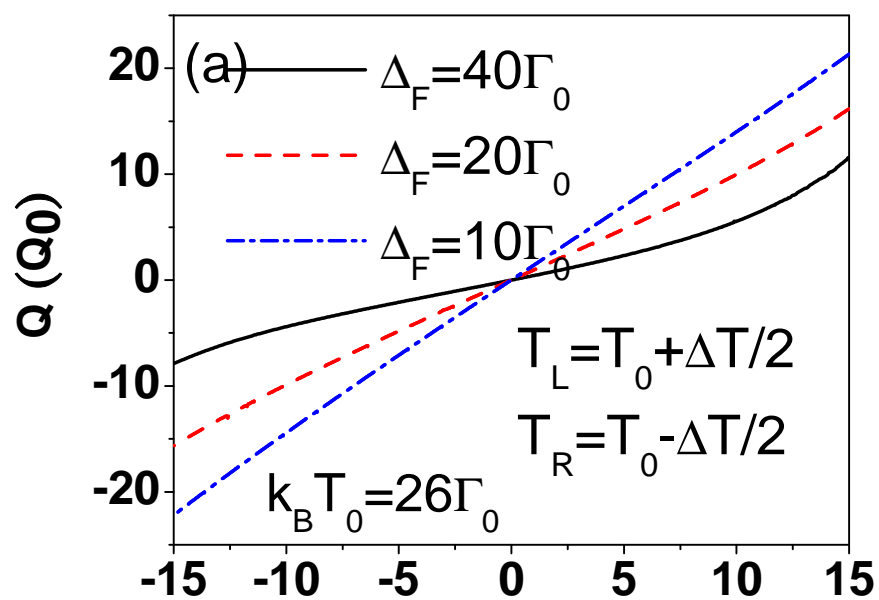


Fig4

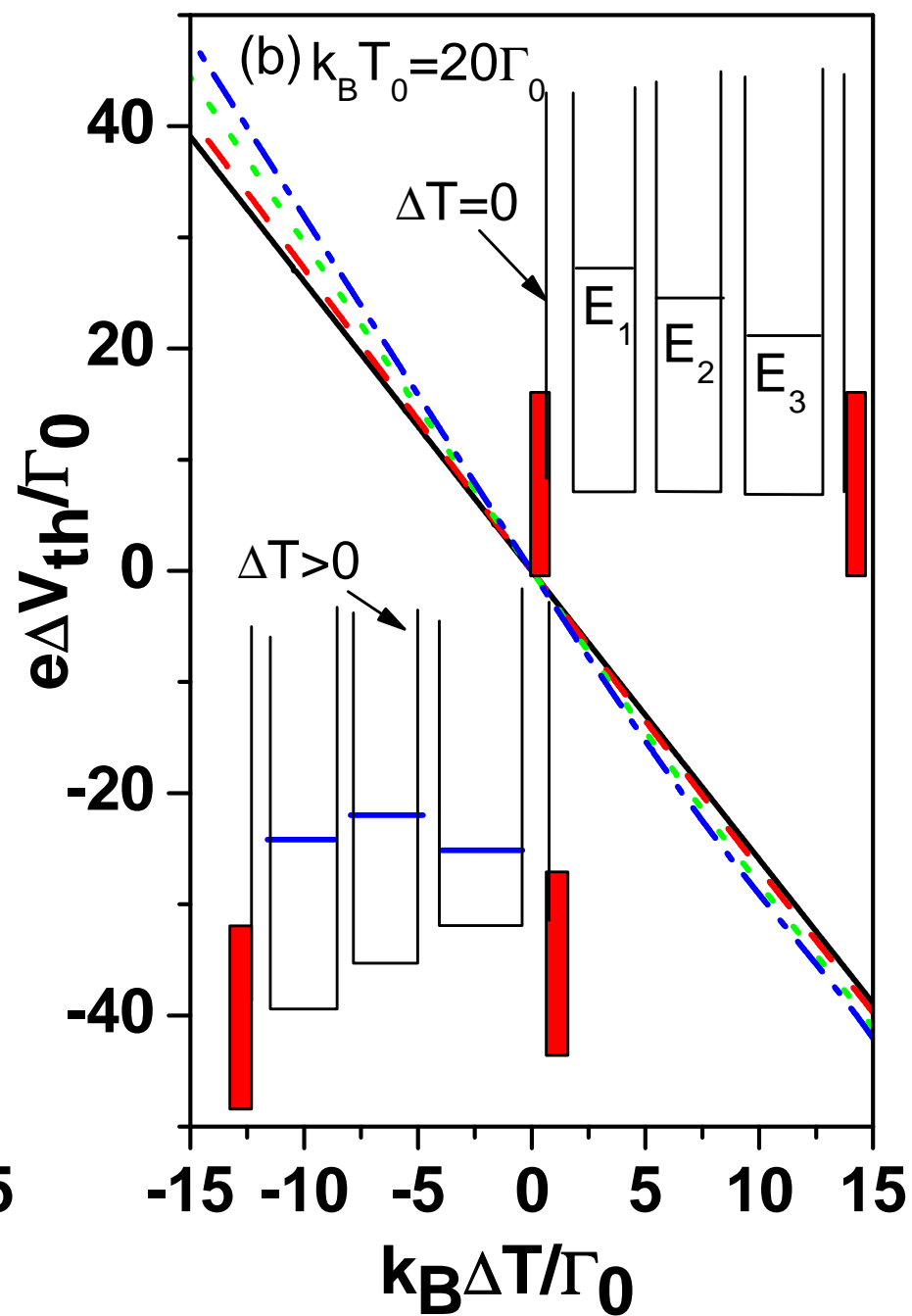
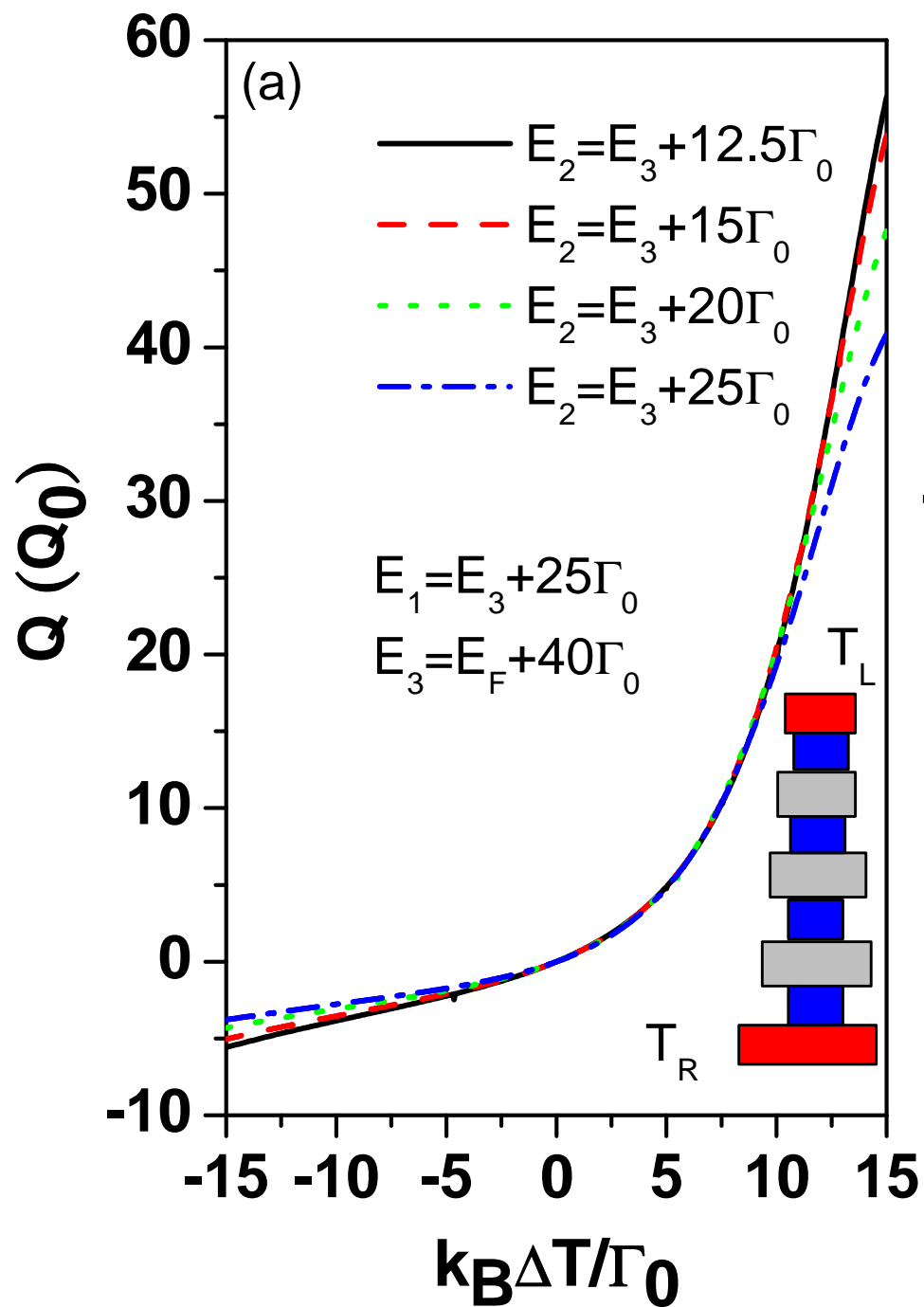


Fig5